14 Mechanical Spectroscopy

14.1 General Remarks

The discoveries of thermally-activated anelastic relaxation processes in solids by Snoek [1], Zener [2, 3] and Gorski [4] were made more than half a century ago. Since then, anelastic measurements have become an established tool for the study of atomic movements in solids. *Relaxation methods* and the closely related *internal friction (or damping)* methods make use of the fact that atomic motion in a solid can be induced by the application of constant or oscillating mechanical stress. Nowadays, anelastic measurements are also denoted by the title *mechanical spectroscopy*.

Under the influence of an applied stress or strain, an instantaneous elastic effect (Hooke's law) is observed, followed by strain or stress which varies with time. The latter effect is called *anelasticity* or *anelastic relaxation*. Anelastic behaviour is reversible. If stress (strain) is removed the sample will return – after some time – to its initial shape. This distinguishes anelastic from plastic behaviour.

Light interstitials, such as H, C, N, and O as well as substitutional solutes and solute-defect complexes are accompanied by local straining of the surrounding lattice. The presence of microstrains surrounding a diffusing atom allows interaction between a macroscopic stress field arising from external forces applied to the material. This interaction generates a rich variety of stress-assisted diffusion effects. Stress-mediated motion can cause time-dependent anelastic (recoverable) strains that result in several types of internal friction processes encountered in many materials.

Sometimes, anelastic relaxation involves the reorientation of point defects which act as elastic dipoles as illustrated in Fig. 14.1. Reorientation relaxations are short-range processes, which in some cases involve only one or few atomic jump(s). However, only in some special cases, exemplified by Snoek relaxation, the same jump produces both reorientation and diffusion. Only then, a simple relationship exists between the relaxation time and the long-range diffusion coefficient. Long-range diffusion controls the so-called Gorski relaxation illustrated in Fig. 14.2. Gorsky relaxation can be produced by bending a sample containing defects, which act as dilatation centers. In practice, the only experimentally known example of Gorski relaxation is due to hydrogen diffusion metals. It can be observed because hydrogen diffusion is very fast.

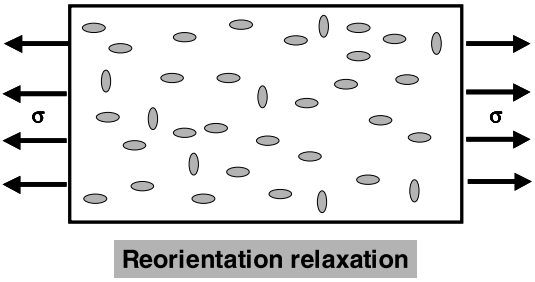

Fig. 14.1. Schematic illustration of anelastic relaxation caused by reorientation of elastic dipoles (represented by *grey ellipses*)

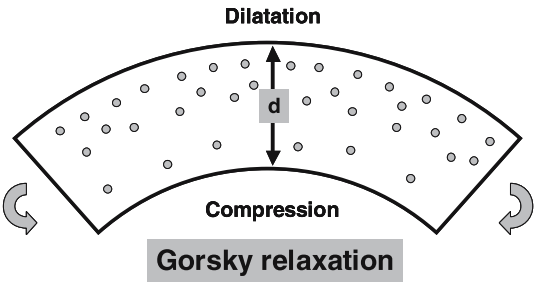

Fig. 14.2. Schematic illustration of Gorski-effect

One should, however, keep in mind that mechanical relaxation and internal friction may arise from various sources. These can range from point-defect reorientations, long-range diffusion, dislocation effects, grain-boundary processes, and phase transformations to visco-elastic behaviour and plastic deformation. Some point-defect relaxations are diffusion-related, some are not. For point-defect relaxations of trapped and paired defects, the nature and the activation enthalpy of the reorientation jump can be significantly different from those associated with long-range diffusion. A review of the substantial body of work that has been accumulated on the study of atomic movement by anelastic methods is beyond the scope of this chapter.

Several textbooks, e.g., those of Zener [3] and Nowick and Berry [5] and reviews by Berry and Pritchet [6, 7] are available for the interested reader. A review about the potential of mechanical loss spectroscopy for inorganic glasses and glass ceramics has been given by Roling [8]. A comprehensive treatment of magnetic relaxation effects can be found in a textbook of Kronmüller [9].

In the present chapter, we first mention the basic concepts of mechanical loss spectroscopy, i.e. of anelastic behaviour and internal friction. Then, we describe some examples of diffusion-related anelasticity such as the *Snoek effect*, the *Zener effect*, the *Gorski effect*, and give an example of a mechanical loss spectrum of glasses.

14.2 Anelasticity and Internal Friction

From the viewpoint of mechanical stress-strain behaviour, we may regard an ideal solid as one which obeys Hooke's law and thus behaves in an ideally elastic manner. Such a solid would always recover completely and instantaneously on removal of an applied stress. If set into vibration, the solid would vibrate forever with undiminished amplitude if totally isolated from its surroundings. The mechanical behaviour of real solids at low stress levels (below the yield stress) is modified by the appearance of anelasticity, which develops at a rate controlled by the atomic movements. It can often be traced back to the presence of mobile atoms or point defects.

A quantitative description of the anelastic behaviour of materials can be found by analysing a model having the name *standard linear solid*, which was originally proposed by Voigt [10] and by Poynting and Thomson [11]. In this model, stress σ, strain ϵ, and their respective time derivatives, $\dot{\sigma}$ and $\dot{\epsilon}$, are related through a linear response equation:

$$\sigma + \tau_\epsilon \dot{\sigma} = M_R(\epsilon + \tau_\sigma \dot{\epsilon})\,. \tag{14.1}$$

This anelastic equation of state is a generalisation of Hooke's law of linear elasticity. Equation (14.1) contains three material parameters: the *strain relaxation time* τ_ϵ, the *stress relaxation time* τ_σ (sometimes also denoted as the stress retardation time), and the *relaxed elastic modulus* M_R. Figure 14.3 illustrates in its left part the strain response of a standard linear solid induced by an instantaneous application and subsequent removal of a constant stress. The continued relaxation of the strain after removal of the stress is also termed the *elastic aftereffect*. The stress response induced by instantaneous application and removal of strain is illustrated in the right part. Note that τ_σ and τ_ϵ are different. It is obvious from Eq. (14.1) that for vanishing time derivatives Eq. (14.1) reduces to Hooke's law. Under uniaxial stress M_R is termed the Young modulus, whereas under applied shear M_R is termed the shear modulus.

Periodic Stress and Strain: Let us now suppose that a uniaxial, periodic stress-time function of frequency ω and amplitude σ_0 of the form

$$\sigma = \sigma_0 \exp\left[i\omega t\right] \tag{14.2}$$

is imposed on the material. The time-dependent strain response of an anelastic solid then is

$$\epsilon = \epsilon_0 \exp\left[i(\omega t - \delta)\right]\,, \tag{14.3}$$

where δ is the phase shift between σ and ϵ. For a completely elastic material, σ and ϵ are in phase and the phase shift is zero for all frequencies. The stress-strain behaviour for an anelastic material under periodic stress is illustrated in Fig. 14.4. For an anelastic material a hysteresis loop is obtained. The area

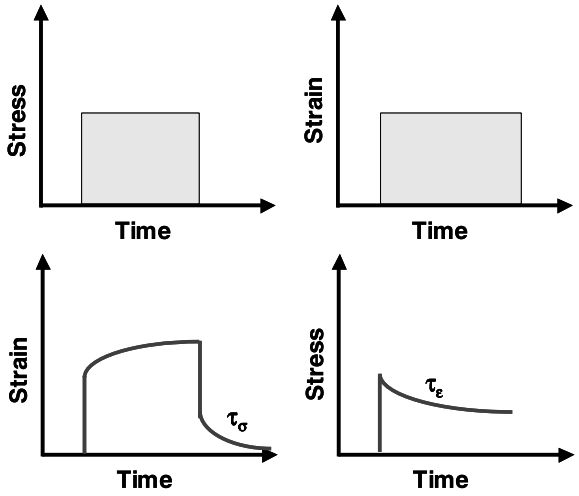

Fig. 14.3. Schematic illustration of anelastic behaviour. The strain response for an instantaneous stress-time function is shown in the *left half*. The stress response for an instantaneous strain-time function corresponds to the *right half*

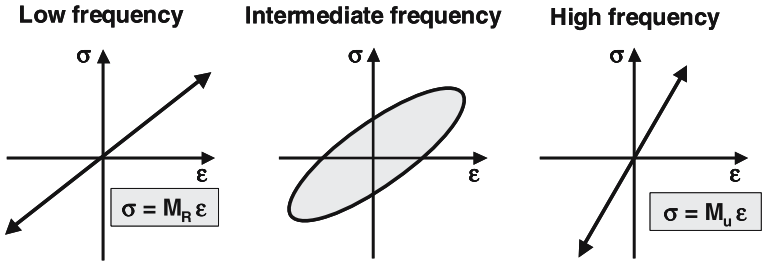

Fig. 14.4. Stress-strain relations for a periodically driven anelastic material at three different frequencies

inside the hysteresis represents the dissipated energy per unit volume and per cycle (see below).

It is convenient to introduce a *complex elastic modulus* $\hat{M}$ via

$$\sigma = \hat{M}\epsilon, \tag{14.4}$$

which can be split up according to

$$\hat{M} = M' + iM'', \tag{14.5}$$

i.e. into real and imaginary parts M' and M'', respectively. Assuming periodic strain with a frequency ω and substituting Eqs. (14.4) and (14.5) into Eq. (14.1) yields after a few steps of algebra

$$\hat{M} = M_R \frac{1 + \tau_\sigma i\omega}{1 + \tau_\epsilon i\omega}\,. \tag{14.6}$$

After separation into real and imaginary parts we get

$$M'(\omega) \; = M_R \frac{1+\tau_\epsilon \tau_\sigma \omega^2}{1+\omega^2\tau_\epsilon^2} = M_R + \Delta M \frac{\omega^2\tau_\epsilon^2}{1+\omega^2\tau_\epsilon^2} \tag{14.7}$$

and

$$M''(\omega) = M_R \frac{(\tau_\sigma - \tau_\epsilon)\omega}{1+\omega^2\tau_\epsilon^2} = \Delta M \frac{\omega\tau_\epsilon}{1+\omega^2\tau_\epsilon^2}\,, \tag{14.8}$$

where the abbreviations

$$\Delta M \;\equiv\; M_U - M_R \quad \text{and} \quad \Delta \;\equiv\; \Delta M/M_R \tag{14.9}$$

have been introduced. At high frequencies, the time scale for stress and strain removals becomes small compared to the relaxation times. Then M' approaches an *unrelaxed elastic modulus*

$$M_U = \frac{M_R \tau_\sigma}{\tau_\epsilon}\,, \tag{14.10}$$

which denotes the stress increment per unit strain at high frequency. Note that M_U and M_R are different because τ_σ and τ_ϵ are different. The tangent of the *loss angle* δ is given by

$$\tan\delta \;\equiv M''/M' = \Delta M \frac{\omega\tau_\epsilon}{M_R + M_U\omega^2\tau_\epsilon^2} \;\equiv\; \Delta \frac{\omega(\tau_\sigma - \tau_\epsilon)}{1+\tau_\sigma\tau_\epsilon\omega^2}\,. \tag{14.11}$$

Internal Friction: Internal friction is the dissipation of mechanical energy caused by anelastic processes occurring in a strained solid. The internal friction, usually called Q^{-1}, in a cyclically driven anelastic solid is defined as

$$Q^{-1} \;\equiv\; \frac{\Delta E_{dissipated}}{E_{stored}}\,, \tag{14.12}$$

where $\Delta E_{dissipated}$ is the energy dissipated as heat per unit volume of the material over one cycle. E_{stored} denotes the peak elastic energy stored per unit volume. For a periodically strained solid subject to sinusoidal stress, the internal friction is given by the following ratio of energy integrals:

$$Q^{-1} = \frac{\int_0^{2\pi} \sigma(\omega t)\dot{\epsilon}(\omega t)_{out-of-phase}\mathrm{d}(\omega t)}{\int_0^{2\pi} \sigma(\omega t)\dot{\epsilon}(\omega t)_{in-phase}\mathrm{d}(\omega t)}\,. \tag{14.13}$$

Substituting the out-of-phase and in-phase components of the strain rate $\dot{\epsilon}$ yields after some algebra the following relation between internal friction and the tangent of the loss angle:

$$Q^{-1} = \pi \tan\delta\,. \tag{14.14}$$

It is convenient to combine the stress and strain relaxation times to a *mean relaxation time* τ, which is defined as the geometric mean of the two fundamental times:

$$\tau \equiv \sqrt{\tau_\sigma \tau_\epsilon}\,. \tag{14.15}$$

We will see later that τ sometimes can be associated with atomic jump processes occurring in the strained solid, having a well-defined activation enthalpy. It is also convenient to combine the relaxed and the unrelaxed moduli to a *mean modulus* M via

$$M \equiv \sqrt{M_R M_U} = \sqrt{\frac{\tau_\sigma}{\tau_\epsilon}} M_R = \sqrt{\frac{\tau_\epsilon}{\tau_\sigma}} M_U\,. \tag{14.16}$$

Using the definitions of the mean modulus Eq. (14.16), the mean relaxation time Eq. (14.15) and Eq. (14.11), yields a basic expression for internal friction:

$$Q^{-1} = \pi \tan\delta \;=\; \pi \frac{\Delta M}{M} \frac{\omega\tau}{1+\omega^2\tau^2}\,. \tag{14.17}$$

The term $\pi\Delta M/M$ is called the *relaxation strength*. The second term describes the frequency dependence of internal friction. Figure 14.5 shows a diagram of Q^{-1} *versus* the logarithm of $\omega\tau$. The frequency-dependent modulus M' is also shown, which varies between the relaxed modulus M_R at low frequencies and the unrelaxed modulus M_U at high frequencies. The maximum of internal friction occurs when

$$\omega\tau = 1 \tag{14.18}$$

is fulfilled. This relation is an important condition for the analysis of anelasticity. If an anelastic solid is strained periodically with a frequency ω the maximum energy loss occurs, when the imposed frequency and relaxation time of the process match.

14.3 Techniques of Mechanical Spectroscopy

Usually, the relaxation time τ is thermally activated according to

$$\tau \;\propto \exp\left(\frac{\Delta H}{k_\mathrm{B} T}\right)\,, \tag{14.19}$$

where ΔH denotes some activation enthalpy. Thus, by varying the temperature at constant frequency ω a maximum of internal friction occurs on the temperature scale. This is the usual way of measuring internal friction peaks, as temperature is easier to vary than frequency. The latter is often more or less fixed by the internal friction device.

By using different experimental techniques, the mechanical loss can be determined at frequencies roughly between 10^{-5} and 5×10^{10} Hz. It is convenient to perform temperature-dependent measurements at fixed frequencies.

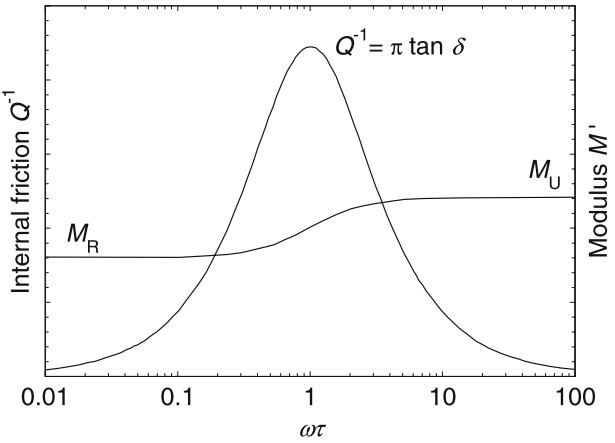

Fig. 14.5. Internal friction, $Q^{-1} = \pi \tan \delta$, and frequency dependent modulus, M', as functions of $\omega\tau$

In this case, a thermally activated process manifests itself in a loss peak, which shifts to higher temperatures as the frequency is increased. Information on the activation enthalpy is then obtained from the peak temperatures, T_{peak}, shifting with frequencies ω by using the equation:

$$\Delta H = -k_{\mathrm{B}} \frac{d \ln \omega}{d(1/T_{peak})} \,. \tag{14.20}$$

In the Hz regime *torsional pendulums* operating at their natural frequencies can be used. A major disadvantage of this technique is that the range of available frequencies is very narrow, often less than half a decade. This makes it difficult to determine accurate values of the activation enthalpies and to analyse frequency-temperature relations in detail. In order to overcome this limitation devices with *forced oscillations* are in use. The frequency window of this technique ranges approximately from 30 Hz up to 10^5 Hz.

At higher frequencies, the mechanical loss of solids can be studied by resonance methods [14, 15]. At even higher frequencies, in the MHz and GHz regimes, ultrasonic absorption and Brillouin light scattering can be used. However, most mechanical loss studies have been done and are still done with the help of low-frequency methods.

Starting in the 1990s, there have been efforts to make use of commercially available instrumentation for dynamic mechanical thermal analysis (DMTA) These devices usually operate in the three-point-bending mode. Among other systems, this technique has been applied to study relaxation processes in oxide glasses [16–18].

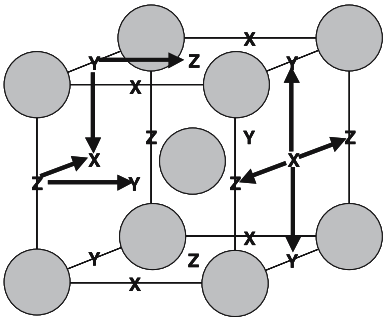

Fig. 14.6. Octahedral interstitial sites in the bcc lattice

14.4 Examples of Diffusion-related Anelasticty

14.4.1 Snoek Effect (Snoek Relaxation)

The Snoek effect is the stress-induced migration of interstitials such as C, N, or O in bcc metals. Although effects of internal friction in bcc iron were reported as early as the late 19th century, this phenomenon was first carefully studied and analysed by the Dutch scientist Snoek [1]. Interstitial solutes in bcc crystals usually occupy octahedral interstitial sites illustrated in Fig. 14.6. Octahedral sites in the bcc lattice have tetragonal symmetry inasmuch the distance from an interstitial site to neighbouring lattice atoms is shorter along $\langle 100 \rangle$ than along $\langle 110 \rangle$ directions. The microstrains surrounding interstitial solutes have tetragonal symmetry as well, which is lower than the cubic symmetry of the matrix. Another way of expressing this is to say that interstitial solutes give rise to permanent elastic dipoles.

Figure 14.6 illustrates the three possible orientations of octahedral sites denoted as X-, Y-, and Z-sites. Without external stress all sites are energetically equivalent, i.e. $E_X = E_Y = E_Z$, and the population n_j^0 of interstitial sites by solutes is $n_X^0 = n_Y^0 = n_Z^0 = n^0/3$. n^0 denotes the total number of interstitials. If an external stress is applied this degeneracy is partly or completely removed, depending on the orientation of the external stress. For example, with uniaxial stress in the Z-direction Z-sites are energetically slightly different from X- and Y-sites, i.e. $E_Z \neq E_X = E_Y$. In contrast, uniaxial stress in $\langle 111 \rangle$ direction does not not remove the energetic degeneracy, because all sites are energetically equivalent. In thermodynamic equilibrium the distribution of interstitial solutes on the X-, Y-, and Z-sites is given by

$$n_i^{eq} = n^0 \frac{\exp(-E_i/k_\mathrm{B}T)}{\sum_{j=X,Y,Z} \exp(-E_j/k_\mathrm{B}T)} \,. \tag{14.21}$$

In general, under the influence of a suitable oriented external stress the 'solute dipoles' reorient, if the interstitial atoms have enough mobility. This redistribution gives rise to a strain relaxation and/or to an internal friction peak.

The relaxation time or the frequency/temperature position of the internal friction peak can be used to deduce information about the mean residence time of a solute on a certain site.

In order to deduce this information, we consider the temporal development of interstitial subpopulations n_X, n_Y, n_Z on X-, Y-, and Z-sites. Suppose that uniaxial stress is suddenly applied in Z-direction. This stress disturbs the initial equipartition of interstitials on the various types of sites and redistribution will start. Fig 14.6 shows that every X-site interstitial that performs a single jump ends either on a Y- or on a Z-site. Interstitials on Y- and Z-sites jump with equal probabilities to X-sites. The rate of change of the interstitial subpopulations can be expressed in terms of the interstitial jump rate, Γ_{int}, as follows:

$$\frac{\mathrm{d}n_X}{\mathrm{d}t} = -2\Gamma_{int} n_X + \Gamma_{int}(n_Y + n_Z)\,. \tag{14.22}$$

The first term on the right-hand side in Eq. (14.22) represents the loss of interstitials located at X-sites due to hops to either Y- or Z-sites. The second term on the right-hand side represents the gain of interstitials at X-sites from other interstitials jumping from either Y- or Z-sites. Corresponding equations are obtained for n_Y and n_Z by cyclic permutation of the indices. Since the total number of interstitials, n^0, is conserved, we have

$$n^0 = n_X + n_Y + n_Z\,. \tag{14.23}$$

Substitution of Eq. (14.23) into Eq. (14.22) yields

$$\frac{\mathrm{d}n_X}{\mathrm{d}t} = -\Gamma_{int} n_X + \frac{\Gamma_{int}}{2}(n^0 - n_X^{eq}) = -\frac{3}{2}\Gamma_{int}\left(n_X - n^0/3\right)\,. \tag{14.24}$$

Equation (14.24) is an ordinary differential equation for the population dynamics of interstitial solutes. Its solution can be written in the form

$$n_X(t) = n_X^{eq} + \left(n_X^0 - n_X^{eq}\right)\exp\left(-\frac{t}{\tau_R}\right)\,, \tag{14.25}$$

where the relaxation time τ_R is given by

$$\tau_R = \frac{2}{3\Gamma_{int}}\,. \tag{14.26}$$

The relaxation time is closely related to the mean residence time, $\bar{\tau}$, of an interstitial solute on a given site. Because an interstitial solute on an octahedral site can leave its site in four directions with jump rate Γ_{int}, we have

$$\bar{\tau} = \frac{1}{4\Gamma_{int}}\,. \tag{14.27}$$

The solute jump rate can be written in the form

$$\Gamma_{int} = \nu^0 \exp\left(-\frac{H^M_{int}}{k_\mathrm{B}T}\right) , \tag{14.28}$$

where ν^0 and H^M_{int} denote attempt frequency and activation enthalpy of a solute jump. Then, the relaxation time of the Snoek effect is

$$\tau_R = \frac{4}{3}\bar{\tau} = \frac{1}{6\nu^0} \exp\left(\frac{H^M_{int}}{k_\mathrm{B}T}\right) . \tag{14.29}$$

The jump of an interstitial solute which causes Snoek relaxation and the elementary diffusion step (jump length $d = a/2$, a = lattice parameter) are identical. The diffusion coefficient developed from random walk theory for octahedral interstitials in the bcc lattice is given by

$$D = \frac{1}{6}\Gamma_{int} d^2 = \frac{1}{24}\Gamma_{int} a^2 . \tag{14.30}$$

Substituting Eqs. (14.27) and (14.29) into Eq. (14.30) yields

$$D = \frac{1}{36}\frac{a^2}{\tau_R} . \tag{14.31}$$

This equation shows that Snoek relaxation can be used to study diffusion of interstitial solutes in bcc metals by measuring the relaxation time. It is also applicable to interstitial solutes in hcp metals since the non-ideality of the c/a-ratio gives rise to an asymmetry in the octahedral sites. Very pure and very dilute interstitial alloys must be used, if the Snoek effect of isolated interstitials is in focus. Otherwise, solute-solute or solute-impurity interactions could cause complications such as broadening or shifts of the internal friction peak.

Figure 14.7 shows an Arrhenius diagram of carbon diffusion in α-iron. For references the reader may consult Le Claire's collection of data for interstitial diffusion [12] and/or a paper by da Silva and McLellan [13]. The data above about 700 K have been obtained with various direct methods including diffusion-couple methods, in- and out-diffusion, or thin layer techniques. The data below about 450 K were determined with indirect methods, including internal friction, elastic after-effect, or magnetic after-effect measurements. The data cover an impressive range of about 14 orders of magnitude in the carbon diffusivity. Extremely small diffusivities around $10^{-24}\,\mathrm{m^2\,s^{-1}}$ are accessible with the indirect methods, illustrating the potential of these techniques. The Arrhenius plot of C diffusion is linear over a wide range at lower temperatures. There is some small positive curvature at higher temperatures. One possible origin of this curvature could be an influence the magnetic transition, which takes place at the Curie temperature T_C. In the case of self-diffusion of iron this influence is well-studied (see Chap. 17).

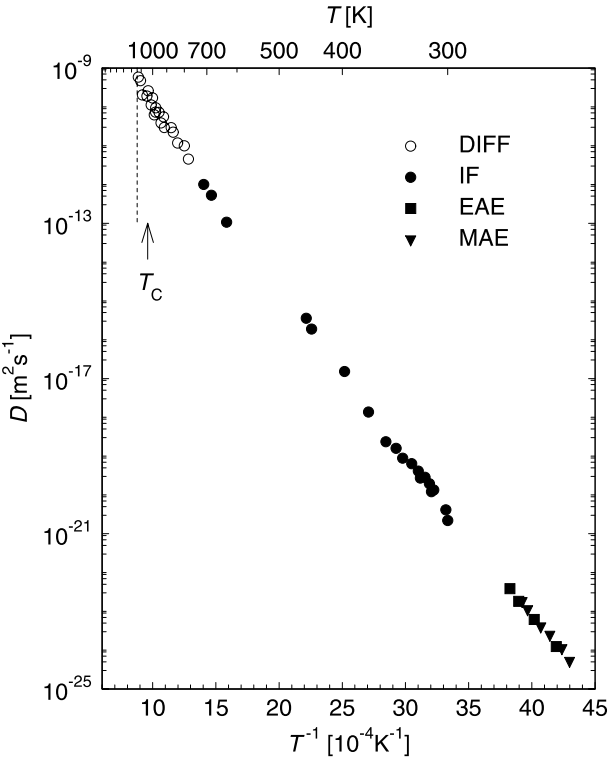

Fig. 14.7. Diffusion coefficient for C diffusion in α-Fe obtained by direct and indirect methods: DIFF = in- and out-diffusion or diffusion-couple methods; IF = internal friction; EAE = elastic after effect, MAE = magnetic after effect

It is interesting to note that the Snoek effect cannot be used to study interstitial solutes in fcc metals. Interstitial solutes in fcc metals are also incorporated in octahedral sites. In contrast to octahedral sites in the bcc lattice, which have tetragonal symmetry, octahedral sites in the fcc lattice and the microstrains associated with an interstitial solute in such sites have cubic symmetry. Interstitial solutes produce some lattice dilation but no elastic dipoles. Therefore, an external stress will not result in changes of the interstitial populations in an fcc matrix.

14.4.2 Zener Effect (Zener Relaxation)

The Zener effect, like the Snoek effect, is a stress-induced reorientation of elastic dipoles by atomic jumps. Atom pairs in substitutional alloys, pairs of interstitial atoms, solute-vacancy pairs possessing lower symmetry than the lattice can form dipoles responsible for Zener relaxation. For example, in strain-free dilute substitutional fcc alloys solute atoms are distributed ran-

domly and isotropically. Solute-solute pairs on nearest-neighbour sites are uniformly distributed among the six ⟨110⟩ directions. The size difference between solute and solvent atoms causes pairs to create microstrains with strain fields of lower symmetry than that of the cubic host crystal.

A well-studied example of solute-solute pair reorientation in fcc materials was reported already by Zener [2]. He observed a strong internal friction peak in Cu-Zn alloys (α-brass) around 570 K. The stress-mediated reorientation of random Zn-Zn pairs along ⟨110⟩ in fcc crystals is somewhat analogous to the Snoek effect. Le Claire and Lomer interpreted this relaxation on the basis of changing directional short-range order under the influence of external stress. In reality, the Zener effect in dilute substitutional fcc alloys depends on several exchange jump frequencies between solute atoms and vacancies. Therefore, it is difficult to relate the effect to the diffusion of solute atoms in a quantitative manner. A satisfactory model, such as is available for the Snoek effect of dilute interstitial bcc alloys, is not straightforward. The activation enthalpy of the process can be determined. However, in a pair model for low solute concentrations the activation energy is more characteristic of the rotation of the dipoles than of long-range diffusion.

14.4.3 Gorski Effect (Gorski Relaxation)

In contrast to reorientation relaxations discussed above, the *Gorski effect* is due to the long-range diffusion of solutes B which produce a lattice dilatation in a solvent A. This effect is named after the Russian scientist Gorski [4]. Relaxation is initiated, for example, by bending a sample to introduce a macroscopic strain gradient. This gradient induces a gradient in the chemical potential of the solute, which involves the size-factor of the solute and the gradient of the dilatational component of the stress. Solutes redistribute by 'up-hill' diffusion and develop a concentration gradient, as indicated in Fig. 14.2. This transport produces a relaxation of elastic stresses, by the migration of solutes from the regions in compression to those in dilatation. The associated anelastic relaxation is finished when the concentration gradient equalises with the chemical potential gradient across the sample. For a strip of thickness d, the Gorski relaxation time, τ_G, is given by

$$\tau_G = \frac{d^2}{\pi^2 \Phi D_B}\,, \tag{14.32}$$

where D_B is the diffusion coefficient of solute B and Φ is the thermodynamic factor. A thermodynamic factor is involved, because Gorski relaxation establishes a chemical gardient.

Equation (14.32) shows that with the Gorski effect one measures the time required for diffusion of B atoms across the sample. The Gorski relaxation time is a macroscopic one, in contrast to the relaxation time of the Snoek relaxation. If the sample dimensions are known, an absolute value of the

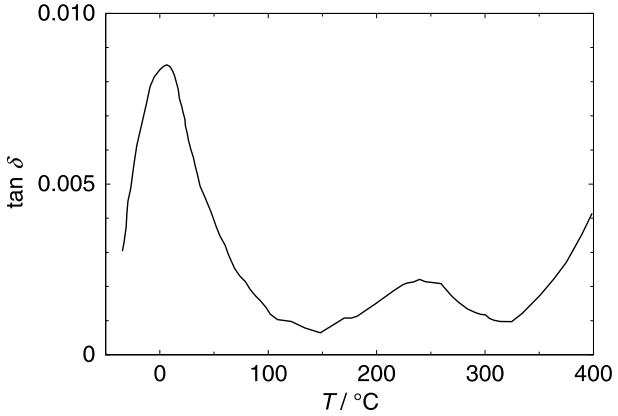

Fig. 14.8. Mechanical loss spectrum of a Na_2O4SiO_4 at a frequency of 1 Hz according to Roling and Ingram [18, 19]

diffusivity is obtained. For a derivation of Eq. (14.32) we refer the reader to the review by Völkl [20]. The Gorski effect is detectable if the diffusion coefficient of the solute is high enough. Gorski effect measurements have been widely used for studies of hydrogen diffusion in metals [6, 20–22].

14.4.4 Mechanical Loss in Ion-conducting Glasses

Diffusion and ionic conduction in ion-conducting glasses is the subject of Chap. 30. Mechanical loss spectroscopy is also applicable for the characterisation of dynamic processes in glasses and glass ceramics. This method can provide information on the motion of mobile charge carriers, such as ions and polarons, as well as on the motion of network forming entities. Mixed mobile ion effects in different types of mixed-alkali glasses, mixed alkali-alkaline earth glasses, mixed alkaline earth glasses, and mixed cation anion glasses. For references see, e.g., a review of Roling [8].

Let us consider an example: Fig. 14.8 shows the loss spectrum of a sodium silicate glass according to Roling and Ingram [18, 19]. Such a spectrum is typical for ion conducting glasses. The low-temperature peak near 0 °C is attributed to the hopping motion of sodium ions, which can be studied by conductivity measurements in impedance spectroscopy and by tracer diffusion techniques as well (for examples see Chap. 30). The activation enthalpy of the loss peak is practically identical to the activation enthalpy of the dc conductivity, which is due to the long-range motion of sodium ions [19]. The intermediate-temperature peak at 235 °C is attributed to the presence of water in the glass. The increase of $\tan\delta$ near 350 °C is caused by the onset of the glass transition.

14.5 Magnetic Relaxation

In ferromagnetic materials, the interaction between the magnetic moment and local order can give rise to various relaxation phenomena similar to those observed in anelasticity. Their origin lies in the induced magnetic anisotropy energy, the theory of which was developed by the French Nobel laureate Neel [24].

An example, which is closely related to the Snoek effect, was reported for the first time in 1937 by Richter [23] for α-Fe containing carbon. The direction of easy magnetisation in α-iron within a ferromagnetic domain is one of the three $\langle 100 \rangle$ directions. Therefore, the octahedral X-, Y-, and Z-positions for carbon interstitials are energetically not equivalent. A repopulation among these sites takes place when the magnetisation direction changes. This can happen when a magnetic field is applied. Suppose that the magnetic susceptibility χ is measured by applying a weak alternating magnetic field. Beginning with a uniform population of the interstitials, after demagnetisation a redistribution into the energetically favoured sites will occur. This stabilises the magnetic domain structure and reduces the mobility of the Bloch walls. As a consequence, a temporal decrease of the susceptibility χ is observed, which can be described by

$$\chi(t) = \chi_0 - \Delta\chi_s \left[1 - \exp\left(-\frac{t}{\tau_R}\right)\right] , \tag{14.33}$$

where $\Delta\chi_s = \chi_0 - \chi(\infty)$ is denoted as the stabilisation susceptibility, t is the time elapsed since demagnitisation, and τ_R is the relaxation time. The relationship between jump frequency, relaxation time, and diffusion coefficient is the same as for anelastic Snoek relaxation.

The magnetic analogue to the Zener effect is directional ordering of ferromagnetic alloys in a magnetic field, which produces an *induced magnetic anisotropy*. The kinetics of the establishment of magnetic anisotropy after a thermomagnetic treatment can yield information about the activation energy of the associated diffusion process. The link between the relaxation time and diffusion coefficient is as difficult to establish as in the case of the Zener effect.

A magnetic analogue to the Gorski effect is also known. In a magnetic domain wall, the interaction between magnetostrictive stresses and the strain field of a defect (such as interstitials in octahedral sites of the bcc lattice, divacancies, etc.) can be minimised by diffusional redistribution in the wall. This diffusion gives rise to a magnetic after-effect. The relaxation time is larger by a factor δ_B/a (δ_B = thickness of the Bloch wall, a = lattice parameter) than for magnetic Snoek relaxation. The variation of the susceptibility with time is more complex than in Eq. (14.33). A comprehensive treatment of magnetic relaxation effects can be found in the textbook of Kronmüller [9]. Obviously, magnetic methods are applicable to ferromagnetic materials at temperatures below the Curie point only.

References

1. J.L. Snoek, Physica **8**, 711 (1941)
2. C. Zener, Trans. AIME **152**, 122 (1943)
3. C. Zener, *Elasticity and Anelasticicty of Metals*, University of Chicago Press, Chicago, 1948
4. W.S. Gorski, Z. Phys. Sowjetunion **8**, 457 (1935)
5. A.S. Nowick, B.S. Berry, *Anelastic Relaxation in Crystalline Solids*, Academic Press, New York, 1972
6. B.S. Berry, W.C. Pritchet, *Anelasticity and Diffusion of Hydrogen in Glassy and Crystalline Metals*, in: *Nontraditional Methods in Diffusion*, G.E. Murch, H.K. Birnbaum, J.R. Cost (Eds.), The Metallurgical Society of AIME, Warrendale, 1984, p.83
7. R.D. Batist, *Mechanical Spectroscopy*, in: *Materials Science and Technology*, Vol. 2B: Characterisation of Materials, R.W. Cahn, P. Haasen, E.J. Cramer (Eds.), VCH, Weinheim, 1994. p. 159
8. B. Roling, *Mechanical Loss Spectroscopy on Inorganic Glasses and Glass Ceramics*, Current Opinion in Solid State Materials Science **5**, 203–210 (2001)
9. H. Kronmüller, *Nachwirkung in Ferromagnetika*, Springer Tracts in Natural Philosophy, Springer-Verlag, 1968
10. W. Voigt, Ann. Phys. **67**, 671 (1882)
11. J.H. Poynting, W. Thomson, *Properties of Matter*, C. Griffin & Co., London, 1902
12. A.D. Le Claire, *Diffusion of C, N, and O in Metals*, Chap. 8 in: *Diffusion in Solid Metals and Alloys*, H. Mehrer (Vol.Ed,), Landolt-Börnstein, Numerical Data and Functional Relationships in Science and Technology, New Series, Group III: Crystal and Solid State Physics, Vol. 26, Springer-Verlag, 1990
13. J.R.G. da Silva. R.B. McLellan, Materials Science and Engineering **26**, 83 (1976)
14. J. Woirgard, Y. Sarrazin, H. Chaumet, Rev. Sci. Instrum. **48**, 1322 (1977)
15. S. Etienne, J.Y. Cavaille, J. Perez, R. Point, M. Salvia, Rev. Sci. Instrum. **53**, 1261 (1982)
16. P.F. Green, D.L. Sidebottom, R.K. Brown, J. Non-cryst. Solids **172–174**, 1353 (1994)
17. P.F. Green, D.L. Sidebottom, R.K. Brown, J.H. Hudgens, J. Non-cryst. Solids **231**, 89 (1998)
18. B. Roling, M.D. Ingram, Phys. Rev. **B 57**, 14192 (1998)
19. B. Roling, M.D. Ingram, Solid State Ionics **105**, 47 (1998)
20. J. Völkl, Ber. Bunsengesellschaft **76**, 797 (1972)
21. J. Völkl, G. Alefeld, in: *Hydrogen in Metals I*, G. Alefeld, J. Völkl (Eds.), Topics in Applied Physics **28**, 321 (1978)
22. H. Wipf, *Diffusion of Hydrogen in Metals*, in: *Hydrogen in Metals III*, H. Wipf (Ed.), Topics in Applied Physics **73**, 51 (1995)
23. G. Richter, Ann. d. Physik **29**, 605 (1937)
24. L. Neel, J. Phys. Rad. **12**, 339 (1951); J. Phys. Rad. **13**, 249 (1952); J. Phys. Rad. **14**, 225 (1954)